REFERENCES AND NOTES

1. M. C. Wilding, B. Harte, J. W. Harris, *Proc. 5th Int. Kimberlite Conf.* (1991), p. 456.
2. B. Harte and J. W. Harris, *Mineral. Mag.* **58A**, 384 (1994).
3. J. W. Harris, M. T. Hutchison, M. Hursthouse, M. Light, B. Harte, *Nature* **387**, 486 (1997).
4. E. Ito, E. Takahashi, Y. Matsui, *Earth Planet. Sci. Lett*. **67**, 238 (1984).
5. M. T. Hutchison, B. Harte, J. W. Harris, I. Fitzsimons, *6th Int. Kimberlite Conf.* (abstr.) (1995), p. 242.
6. To obtain adequate count rates, the conventional Mössbauer source (typical specific activity 100 mCi/cm^2) is replaced by a point source (specific activity $>$ 2000 mCi/cm^2). The gamma rays are collimated to the selected sample diameter using a Pb shield, and the source-sample distance is reduced to $<$5 mm. The latter results in a solid angle similar to conventional experiments, and hence a similar count rate. Because the signal quality depends on absorber density (measured in milligrams of Fe per square centimeter) and not the total amount of iron in the sample, the reduction in sample size has no effect on the effective thickness of the absorber. When electronic absorption due to heavier elements is low and the point source is relatively new ($<$1 year old), high-quality Mössbauer spectra (comparable to conventional measurements) can be recorded on samples with diameters as small as 100 μm. For further information see C. A. McCammon, V. Chaskar, and G. G. Richards [*Meas. Sci. Technol*. **2**, 657 (1991)] and C. A. McCammon [*Hyper. Int.* **92**, 1235 (1994)].
7. Compositions were determined using a Cameca Camebax electron microprobe at the University of Edinburgh, Department of Geology and Geophysics, operating at 20 kV with a beam current of 20 nA.
8. The epoxy disks were mounted with cellophane tape behind a 200- to 500-μm-diameter hole drilled in 25-μm- thick Ta foil. The foil acts as a collimator, absorbing more than 99% of the 14.4-keV gamma rays. Absorber densities based on the thickness of the samples and chemical compositions were $>$ 10 mg of Fe per square centimeter for the (Mg,Fe)O inclusions, and approximately 1 mg of Fe per square centimeter for the (Mg,Fe,Al)(Si,Al)O_3 and TAPP inclusions. Mössbauer spectra were collected for times ranging from 1 day for the (Mg,Fe)O inclusions to more than 20 days for the silicate inclusions. Mössbauer spectra were recorded at room temperature in transmission mode on a constant acceleration Mössbauer spectrometer with a nominal 20 mCi of ^{57}Co high specific activity source (2 Ci/cm^2) in a 12-μm Rh matrix. The velocity scale was calibrated relative to 25-μm α-Fe foil using the positions certified for National Bureau of Standards standard reference material no. 1541; line widths of 0.42 mm/s for the outer lines of α-Fe were obtained at room temperature. The spectra were fitted to Lorentzian and Voigt line shapes using the commercially available fitting program NORMOS written by R.A. Brand (distributed by Wissenschaftliche Elektronik GmbH, Germany).
9. V. V. Kurash *et al*., *Inorg. Mater.* **8**, 1395 (1972).
10. We fitted Mössbauer spectra of (Mg,Fe)O to two Fe^{2+} doublets and one Fe^{3+} singlet, all with Voigt line shape. The area of Fe^{3+} absorption is constrained by the asymmetry of the main doublet, and is therefore relatively independant of the fitting model.
11. C. A. McCammon, J. W. Harris, B. Harte, M. T. Hutchison, in *Plume 2*, D. L. Anderson, S. R. Hart, A. W. Hofmann, Eds. [*Terra Nostra* **3**, 91 (1995)].
12. F. Seifert, B. O. Mysen, D. Virgo, E.-R. Neumann, *Annu. Rep. Carneg. Inst. Wash. Geophys. Lab*. **81**, 355 (1982).
13. H. Annersten, M. Olesch, F. A. Seifert, *Lithos* **11**, 301 (1978).
14. Y. B. Wang, F. Guyot, R. C. Liebermann, *J. Geophys. Res.* **97**, 12, 327 (1992).
15. C. A. McCammon, *Phase Trans.* **58**, 1 (1996); G. M. Bancroft, A. G. Maddock, R. G. Burns, *Geochim. Cosmochim. Acta* **31**, 2219 (1967).
16. C. A. McCammon, *Nature* **387**, 694 (1997).
17. D. H. Speidel, *J. Am. Ceram. Soc.* **50**, 243 (1967).
18. M. Brearly, *J. Geophys. Res.* **B10**, 15703 (1990).
19. B. J. Wood and D. C. Rubie, *Science* **273**, 1522 (1996).
20. T. Irifune and M. Isshiki, paper presented at the International Conference on High-Pressure Science and Technology (AIRAPT-16 and HPCJ-38), Kyoto, Japan (1997), p. 169.
21. R. O. Moore, M. L. Otter, R. S. Rickard, J. W. Harris, J. J. Gurney, *Geol. Soc. Aust. Abstr.* **16**, 409 (1986).
22. F. Guyot, M. Madon, J. Peyronneau, J. P. Poirier, *Earth Planet. Sci. Lett.* **90**, 52 (1988); Y. Fei, H. K. Mao, B. O. Mysen, *J. Geophys. Res*. **96**, 2157 (1991); S. E. Kesson and J. D. Fitz Gerald, *Earth Planet. Sci. Lett.* **111**, 229 (1991).
23. S. Lauterbach, C. A. McCammon, F. Seifert, paper presented at the 75th annual meeting of the German Mineralogical Society, Cologne, Germany, 15 to 19 September 1997.
24. M. Hutchinson, in preparation.

25. The mineral inclusions were supplied by B. Harte, and the electron microprobe analyses for samples BZ66, BZ67, BZ73, and BZ210B were performed by M. Wilding and B. Harte. The manuscript was improved through discussions with B. Harte and S. Kesson.

3 July 1997; accepted 18 August 1997

Triton's Distorted Atmosphere

J. L. Elliot,* J. A. Stansberry, C. B. Olkin, M. A. Agner, M. E. Davies

A stellar-occultation light curve for Triton shows asymmetry that can be understood if Triton's middle atmosphere is distorted from spherical symmetry. Although a globally oblate model can explain the data, the inferred atmospheric flattening is so large that it could be caused only by an unrealistic internal mass distribution or highly supersonic zonal winds. Cyclostrophic winds confined to a jet near Triton's northern or southern limbs (or both) could also be responsible for the details of the light curve, but such winds are required to be slightly supersonic. Hazes and clouds in the atmosphere are unlikely to have caused the asymmetry in the light curve.

Data from the Voyager 2 encounter with Triton in August 1989 (*1*) showed that Triton's atmosphere is dynamic on short time scales. Dark plumes rose from the surface to an altitude of 8 km and were observed to drift downwind for more than 100 km (*2*). Wind streaks on the surface in the southern hemisphere indicated a northeasterly flow near the ground with wind speeds of 5 to 15 m s^{-1} (*3*). Discrete clouds were seen up to 8 km above the surface, and haze was detected up to altitudes of 20 to 30 km (*4*). Because Triton's predominantly N_2 atmosphere is in vapor-pressure equilibrium with the surface ice (the heat of vaporization and condensation equalize the surface temperature on Triton), seasonal changes in insolation can produce changes in surface pressure of several orders of magnitude (*5*). The thermal structure of Triton's middle atmosphere is probably controlled by a steady-state balance of heat input from the sun and magnetospheric electrons, radiative processes involving CH_4 and CO, and thermal conduction to the surface (*6*). On the basis of the plumes, the lower 8 km of the atmosphere has been modeled as a troposphere (*7*).

To test atmospheric models based on Voyager data and to measure the predicted changes in surface pressure with time, we began monitoring Triton's atmosphere with a series of Earth-based stellar occultation observations in 1993. The results of these observations (*8*) are not consistent with the temperature and pressure predicted by models (*6*) at an altitude of 90 km. For the 14 August 1995 occultation discussed here, the Infrared Telescope Facility (IRTF) was situated close enough to the center of Triton's occultation shadow to record the partial focusing of starlight by Triton's atmosphere—a phenomenon known as the "central flash" (*9*). The central-flash ray-paths probe several scale heights deeper into the atmosphere than the main immersion and emersion light curves of the occultation. They also sample large portions of the planetary limb, making the central flash a tool that has been used to investigate the properties of winds and extinction (particulate and molecular) in the atmospheres of Mars, Saturn, Titan, and Neptune (*10*, *11*).

The visible wavelength occultation data (Fig. 1) exhibit two asymmetries in the light

J. L. Elliot, Department of Earth, Atmospheric, and Planetary Sciences and Department of Physics, Building 54-422, Massachusetts Institute of Technology, 77 Massachusetts Avenue, Cambridge, MA 02139–4307, USA; and Lowell Observatory, 1400 West Mars Hill Road, Flagstaff, AZ 86001–4499, USA.

J. A. Stansberry and C. B. Olkin, Lowell Observatory, 1400 West Mars Hill Road, Flagstaff, AZ 86001–4499, USA.

M. A. Agner, Department of Earth, Atmospheric, and Planetary Sciences, Building 54-314, Massachusetts Institute of Technology, 77 Massachusetts Avenue, Cambridge, MA 02139–4307, USA.

M. E. Davies, RAND Corporation, 1700 Main Street, Santa Monica, CA 90407–3297, USA.

*To whom correspondence should be addressed at the Department of Earth, Atmospheric, and Planetary Sciences, Building 54-422, Massachusetts Institute of Technology, 77 Massachusetts Avenue, Cambridge, MA 02139–4307, USA. E-mail: jle@mit.edu

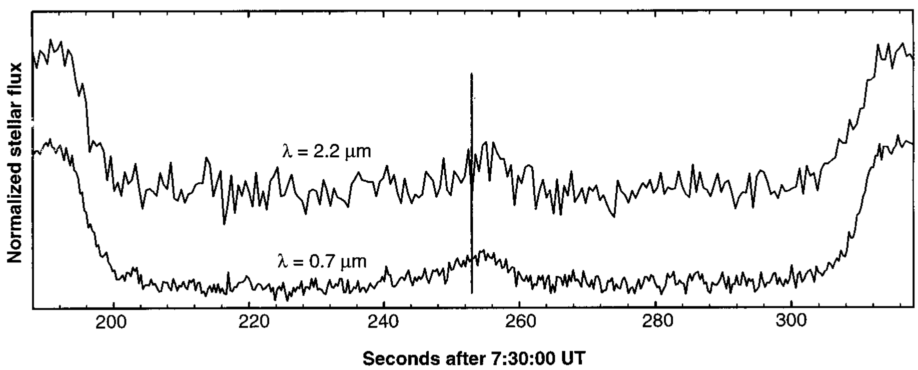

Fig. 1. IRTF light curves for the 14 August 1995 Triton occultation (*8*). The signals from the occulted star are plotted versus time {IR is shown by the upper line [wavelength (λ) = 2.2 μm]; visible light is shown by the lower line (λ = 0.7 μm)}. The solid vertical line indicates the midtime.

curve. (i) The peak of the central flash occurs about 2 s later than the midtime between the half-light times, and (ii) the slope of the light curve is shallower before the peak of the central flash than afterward. The infrared (IR) light curve also shows a delayed peak. We consider two classes of models for explaining these features of the visible light curve: (i) distortion of the refractive properties of the atmosphere from a spherical shape, and (ii) extinction within the atmosphere. In the first class of models, we explore the possibilities that the atmospheric shape is distorted by a nonradial component of Triton's gravitational field and that the shape is oblate because of zonal winds. We also consider the possibility that changes in the refractivity of the atmospheric gas itself (nonuniform composition) could explain the light curve.

To quantify the distortion required to reproduce the measured light curve, we constructed a model atmosphere in which surfaces of constant refractivity were elliptical, with the ellipticity $\varepsilon = 1 - R_p/R_e$, where R_e is the equatorial radius and R_p is the polar radius. For each position along the IRTF path, the points on the limb that supplied refracted starlight are those whose perpendicular from the tangent to the limb intersects the telescope. For each limb point that was a source of refracted starlight, the flux was calculated from a small planet model (*12*), modified to use the radius of curvature (instead of the radius) of the elliptical limb to determine the focusing. Fluxes from all perpendicular limb points were added to obtain the light-curve flux. Figure 2 shows the starlight intensity in the vicinity of the central flash predicted from our best elliptical model for the light curve, and it illustrates how the orientation of the ellipse is related to the timing of the central flash and the different light-curve slopes before and after it. At no time does the IRTF chord cross the evolute, a condition that is in agreement with the lack of a sharp peak in the light curve.

The elliptical model was fit to the IRTF visible light curve by least squares (Table 1). Fits for three cases of atmospheric ellipticity were carried out: a circular model ($\varepsilon = 0$), a prolate model ($\varepsilon < 0$), and an oblate model ($\varepsilon > 0$); the implied atmospheric properties (*13*) were also derived. The orientation of the ellipse was a free parameter. The "minimum radius probed" (Table 1) refers to the deepest level of the atmosphere probed by starlight (from the near limb) for the IRTF data, as calculated for the three models. These can be compared with the surface radius [1352.6 ± 2.4 km (*14*)]. The best-fit oblate model is compared with the data in Fig. 3A. Both the oblate and prolate models match the time offset and differing slopes in the central flash (Fig. 3B), whereas the circular model does not. The best fitting elliptical figures are symmetric about Triton's polar axis [(*15*) Table 1 and Fig. 2]. Assessing the significance of the three solutions with the *F* test [(*16*) Table 1], the oblate solution is the most probable choice of the three.

Assuming that the data are telling us that Triton's atmosphere is oblate, we first examine whether the modeled ellipticity is consistent with an atmospheric circulation. Winds symmetric with Triton's rotation axis are an attractive explanation, because the orientations of the elliptical models (Table 1) were free parameters and are con-

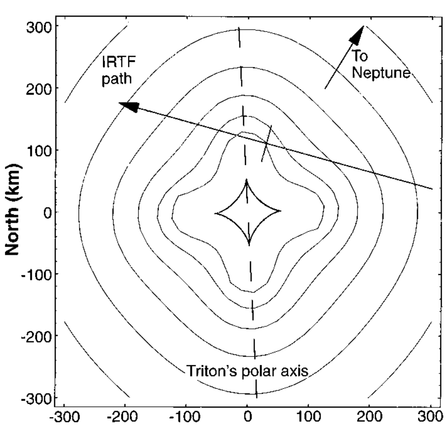

Fig. 2. Starlight contours near the center of Triton's shadow. The model is the oblate solution in Table 1. The contours in the shadow plane denote equal $\log_{10}$ intervals for starlight, between −1.1 and −0.6, and the diamond in the center is the evolute of the central flash (the locus of focal points for an elliptical figure). Triton's polar axis is indicated by the dashed vertical line, and the direction to Neptune is indicated by an arrow. The IRTF path through this shadow begins at the right of the figure and proceeds east by northeast, with the midtime between the immersion and emersion half-light times indicated by the hash mark.

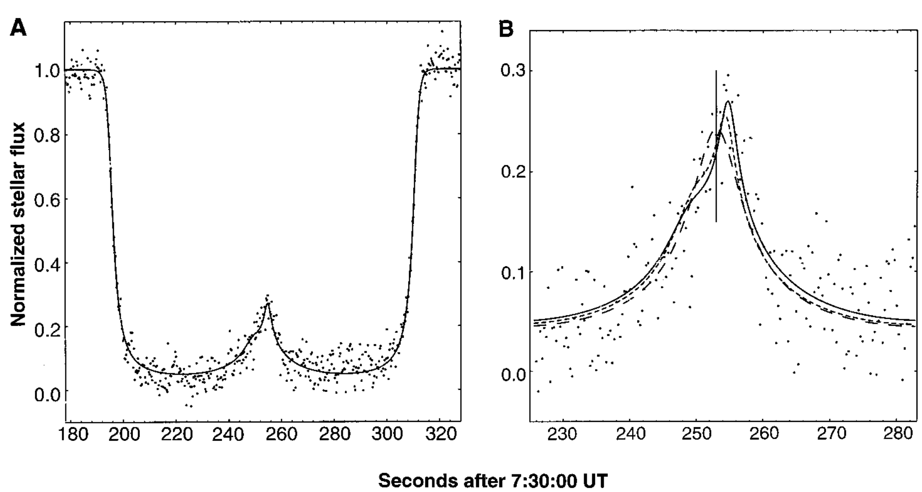

Fig. 3. Light curve and model. (**A**) The data are plotted as points, and the solid line is the best fitting model to the light curve, for an apparent ellipticity of 0.018 (the oblate solution given in Table 1). (**B**) Enlarged view of the central flash region for the circular, prolate, and oblate model fits to the visible light curve. The oblate model is indicated by the solid line, the prolate by the short dashed line, and the circular by the long dashed line. The solid vertical line indicates the midtime (Fig. 1).

sistent with the direction of Triton's pole. The (deprojected) ellipticity of 0.042 requires an equatorial wind speed of 290 m s^{-1}—about twice the speed of sound in Triton's atmosphere and 18 times larger than the tangential velocity of Triton's surface due to its rotation (*17*). Such high-velocity winds are not realistic, but winds restricted to latitude bands near the northern or southern limbs (or both) can explain the data without being so extreme. By specifying an atmospheric pressure gradient that is consistent with the modeled ellipticity of the atmosphere, we can calculate cyclostrophic wind velocities in the region of the atmosphere probed by the central flash; that is, near 45° north or south (*18*). We restricted our attention to a 10° latitude band, specified a constant surface pressure and a constant latitudinal temperature gradient within the band, and assumed that the temperature was constant with altitude. Although the isobars are locally oblate (pressure monotonically declines from the equatorward to the poleward side of the band), isopycs are locally prolate below about 13 km altitude and oblate above (*19*). Based on this simple model, we found that the latitudinal temperature gradient required to achieve a local atmospheric distortion equivalent to an ellipticity of 0.042 was about –0.7 K $degree^{-1}$, with a resulting wind speed at 30 km altitude of 170 m s^{-1} (which is 30 m s^{-1} greater than the sonic velocity). The latitudinal temperature gradient required to give an ellipticity of –0.032 (Table 1) near the surface was –1.5 K $degree^{-1}$, with a corresponding wind speed of 110 m s^{-1} at 5 km altitude (*20*). It is possible that the isopycs in Triton's atmosphere that formed the central flash are oblate near the south limb and prolate near the north, giving an effective pear shape to the atmosphere. If so, both limbs could have contributed flux to the central flash, and the required ellipticities and wind speeds would be less. Such complex atmospheric figures are not unknown: Multiple chords probing Titan's central flash revealed a limb profile more complex than a simple ellipse (*11*).

In principle, it is possible for refractive asymmetry to be caused by nonuniform atmospheric composition. We consider this unlikely because the detected minor constituents, CO and CH_4, have small mixing ratios—less than 1% in the regions probed by Voyager (*21*). Argon would not have been detected by Voyager. However, the winds (*2*, *3*) that are clearly evident from Voyager imagery should keep the atmosphere well mixed. So even if there were substantial amounts of Ar, large refractivity gradients could not be maintained.

Finally, we consider gravity as the cause of the distorted atmosphere. The deviation of a gravity field from spherical symmetry could be produced by a nonspherical mass distribution and could have contributions from four sources: Triton's rotation, tidal forces from Neptune, a nonuniform internal mass distribution, or a permanent distortion in Triton's figure. The ellipticities caused by Triton's rotation and the tidal perturbation of Triton's atmosphere by Neptune, ~0.001 (*22*), are more than 10 times smaller than our modeled ellipticity. Triton's internal mass distribution, or an intrinsically distorted figure for Triton itself, are also unlikely to be

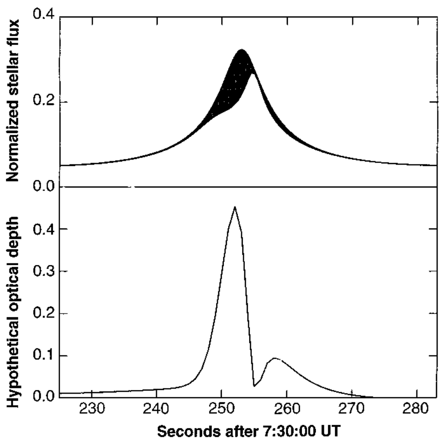

Fig. 4. Minimum optical depth needed for asymmetry. In the upper panel, the lower curve represents the best fitting oblate model, and the upper curve represents a circular model that is everywhere greater than or equal to the lower light curve. The shaded region corresponds to the minimum extinction required to generate the observed light curve from the basic refraction light curve produced by a spherically symmetric atmosphere. The lower panel shows the corresponding optical depth.

Table 1. Models for Triton's atmospheric figure.

	Circular	Prolate	Oblate
	*Fitted parameters**		
Background level (ADU s^{-1})	1,029,670 ± 140	1,029,600 ± 150	1,029,500 ± 160
Background slope (ADU s^{-2})	0.25 ± 0.17	0.26 ± 0.17	0.24 ± 0.17
Star signal (ADU s^{-1})	21,110 ± 140	21,170 ± 150	21,270 ± 160
Midtime (seconds after 07:30:00 UT)	253.00 ± 0.05	253.00 ± 0.05	252.99 ± 0.05
Equatorial half-light radius (km)†	1,445.3 ± 1.4	1,441.4 ± 2.3	1,450.8 ± 1.9
Lambda (isothermal) at half-light	85.8 ± 6.9	84.3 ± 2.3	77.7 ± 4.8
Thermal gradient exponent [*b* (*12*)]	15.6 ± 6.6	12.8 ± 3.8	8.8 ± 4.6
Apparent ellipticity	0	−0.014 ± 0.003	0.018 ± 0.003
Position angle (PA) of pole‡ (degrees)	0	3.7 ± 6.4	2.5 ± 5.2
Minimum center distance (km)	94 ± 11	98 ± 12	115 ± 15
	Derived parameters		
Equatorial ellipticity (deprojected)	0	−0.032 ± 0.007	0.042 ± 0.007
Minimum radius probed (km)	1,382.6 ± 3.7	1,397.8 ± 4.4	1,357.1 ± 7.0
Nominal winds (m s^{-1})§	0	110	170
Number density‖ (10^{14} cm^{-3})	2.77 ± 0.39	2.10 ± 0.30	3.36 ± 0.57
Pressure‖ (μbar)	1.65 ± 0.23	1.27 ± 0.17	2.02 ± 0.28
Temperature‖ (K)	43.2 ± 2.3	43.9 ± 2.4	43.5 ± 2.5
Temperature gradient (*12*)‖ (K km^{-1})	0.48 ± 0.20	0.40 ± 0.19	0.27 ± 0.14
	Fit information		
Degrees of freedom	1,493	1,491	1,491
Sum of squared residuals	9.52583×10^{7}	9.51108×10^{7}	9.43371×10^{7}
F test: probability (circular+noise)	—	9.9×10^{-2}	5.5×10^{-7}

*The shadow velocity was fixed at 25.0341 km s^{-1}, and the time per data point was 0.300 s. †The equatorial radius corresponds to the semimajor axis for the oblate model and to the semiminor axis for the prolate model. ‡PA is measured from north through east; the PA of Triton's pole was 3.2° and the PA of Neptune (relative to the center of Triton) was −32°. §For the prolate model, this represents the cyclostrophic wind speed required to give local ellipticity of −0.032 at 5 km altitude; for the oblate model, this is the cyclostrophic wind at 45° S and 1382-km radius for an atmosphere with local (deprojected) ellipticity of 0.042. ‖For a pure N_2 atmosphere at the radius of 1400 km (*8*).

able to create the necessary distortion. The first-order deviation of Triton's gravity field from spherical symmetry is described by Triton's J_2 coefficient, which was not directly measured during the Voyager flyby. However, a nonuniform mass distribution would reveal itself through distortion of Triton's surface figure. Although only spherical solutions of the surface-feature control network were originally attempted for Triton (*16*), the distorted atmosphere has prompted us to reexamine the original data in an attempt to obtain triaxial solutions for Triton's surface. Unfortunately, the control network covers only 80° in latitude and 120° in longitude, which is too small a fraction of Triton's globe to distinguish a spherical shape from an elliptical shape. Reanalysis of Triton's limb images shows departures from spherical symmetry of no more than ~5 km (*23*). If Triton's figure does have an ellipticity equal to our deprojected value of 0.042, we find that the resulting value of the second-order gravity coefficient J_2 is 0.028. This value is high and probably requires an unrealistic internal mass distribution.

Known hazes and clouds in Triton's atmosphere suggest extinction as an alternative explanation to refraction for the asymmetry of the light curve, but we believe that it is unlikely for two reasons. First, we established the minimum extinction needed to cause the asymmetry in the visible light curve by adjusting the closest approach distance of our circular model until the symmetric curve was everywhere equal to or greater than the best fitting oblate model. The difference between the two curves establishes the minimum extinction needed to account for the asymmetry (Fig. 4). This minimum extinction model yields a minimum center distance for the IRTF chord of only 80 km, which is 2.4 σ smaller than the 145 ± 27 km derived for a circular solution from the chords (*8*). So a spherical extinction model is not self-consistent. Second, we compared the visible and IR light curves to find evidence for extinction. Using the minimum-extinction visible light curve (Fig. 4) and assuming a functional form for the optical depth $\tau(\lambda) = \tau_{vis} (\lambda/\lambda_{vis})^{-n}$, we fit the IR light curve with $\lambda = \lambda_{IR}$ and the signal levels, midtime, and n as free parameters (*24*). The results yield n = –0.39 ± 0.27. We conclude that if extinction caused the asymmetry, then its wavelength dependence between 0.7 and 2.2 μm is different from that observed over a range of visible wavelengths by Voyager [n = 1.8 (*25*)] and different from visible extinction at occultation altitudes for Titan [n ~ 1.9 (*11*)].

Extinction and refraction are not mutually exclusive possibilities, and our models for either one have implications for the other. For example, the minimum radius probed in the spherical refractive model (Table 1) is well above Triton's clouds and probably above the bulk of Triton's very thin hazes, so we would not expect extinction to have affected the light curve if Triton's atmosphere is spherical (and the central flash should have been symmetric and centered within the light curve minimum). On the other hand, the minimum radius probed in the globally oblate model is nominally in the troposphere, where the thickest clouds (τ ≈ 0.1) were observed, so the globally oblate, purely refractive model is probably not self-consistent. In our models where the atmosphere was taken to be distorted only near the northern or southern limbs or both, the minimum radius probed was about 1376 km, which is only 6 km deeper than for the spherical model, so we would not expect to see extinction effects, yet the shape of the atmosphere would explain the light curve; this model at least offers a self-consistent solution, although admittedly requiring extreme winds.

REFERENCES AND NOTES

1. E. C. Stone and E. D. Miner, *Science* **246**, 1417 (1989).
2. B. A. Smith *et al*., *ibid.*, p. 1422; L. A. Soderblom *et al*., *ibid*. **250**, 410 (1990).
3. A. P. Ingersoll, *Nature* **344**, 315 (1990).
4. J. B. Pollack, J. M. Schwartz, K. Rages, *Science* **250**, 440 (1990).
5. J. R. Spencer and J. M. Moore, *Icarus* **99**, 261 (1992); C. J. Hansen and D. A. Paige, *ibid.*, p. 273.
6. R. V. Yelle, J. I. Lunine, D. M. Hunten, *ibid.* **89**, 347 (1991); V. A. Krasnopolsky, B. R. Sandel, F. Herbert, R. J. Vervack, *J. Geophys. Res.* **98**, 3065 (1993); D. F. Strobel and M. E. Summers, in *Neptune and Triton*, D. P. Cruikshank, Ed. (Univ. of Arizona Press, Tucson, AZ, 1995), pp. 1107–1148; D. F. Strobel, X. Zhu, M. E. Summers, M. H. Stevens, *Icarus* **120**, 266 (1996).
7. R. V. Yelle, J. I. Lunine, D. M. Hunten, *Icarus* **89**, 347 (1991).
8. C. B. Olkin *et al*., *ibid.*, in press.
9. J. L. Elliot, E. W. Dunham, C. Church, *Sky Tel.* **52**, 23 (1976).
10. J. L. Elliot *et al*., *Astrophys. J.* **217**, 661 (1977); E. Lellouch, W. B. Hubbard, B. Sicardy, F. Vilas, P. Bouchet, *Nature* **324**, 227 (1986); W. B. Hubbard *et al*., *Astrophys. J.* **325**, 490 (1988); B. Sicardy *et al*., *Nature* **343**, 350 (1990); P. D. Nicholson, C. McGhee, R. G. French, *Icarus* **113**, 57 (1995).
11. W. B. Hubbard *et al*., *Astron. Astrophys.* **269**, 541 (1993).
12. J. L. Elliot and L. A. Young, *Astron. J.* **103**, 991 (1992). This model assumes hydrostatic equilibrium and a power-law temperature dependence on radius r, $T(r) = T_0(r/r_0)^b$, where the temperature is T_0 at a reference radius r_0 and b is the power-law exponent. The refractivity model used here is an elliptical generalization of this model.
13. The atmospheric parameters apply to the subimmersion (longitude 81.9°, latitude –6.0°) and subemersion (longitude 270.5°, latitude 13.5°) half-light points on Triton (*8*). All the fitted global limb shapes give nearly the same temperature (Table 1) for a radius of 1400 km: 43.5 ± 2.5 K for the oblate solution. This agrees within the error with the 44.5 ± 1.8 K temperature derived from models excluding the central flash (*8*), which are about 5 K colder than models based on Voyager data (*6*). The pressure at 1400 km is somewhat dependent on the assumption of limb shape (Table 1), but all pressures are well above the predictions of models based on Voyager data (*6*). Our higher pressure may be due to an inadequacy of the models or to a change in Triton's surface pressure between 1989 and 1995 (*5*).
14. M. E. Davies, P. G. Rogers, T. R. Colvin, *J. Geophys. Res.* **96**, 15 (1991).
15. Triton's atmospheric figure at the half-light level from the occultation chords is $\varepsilon = -0.029$, PA = –20 ± 10 (Table 1), minimum center distance = 191 ± 36 km (*8*). This figure applies to a radius of about 1451 km and applies predominantly to the eastern and western limbs, whereas the light-curve figure is dominated by light from the northern or southern limb that passes through the atmosphere at a smaller radius. Hence the shape of Triton's atmosphere may be changing with altitude (a property of some of the global circulation models we investigated).
16. As described by P. R. Bevington [*Data Reduction and Error Analysis for the Physical Sciences* (McGraw-Hill, New York, 1969)], we add two additional parameters to a least-squares fit and calculate χ_1^2 for the first fit and χ_2^2 for the second fit (with the extra parameters). Then we form the statistic $F_x = (\chi_1^2 - \chi_2^2)/(\chi_2^2/d) = (\Sigma_1 - \Sigma_2)/(\Sigma_2/d)$, where d is the number of degrees of freedom for the second fit, and Σ_1 and Σ_2 are the sum of squared residuals from the first and second fits, respectively. If the noise is assumed to follow a Gaussian distribution, then F_x follows the F distribution, and one can readily calculate the probability that the noise would cause a given value of F_x or larger.
17. Hubbard *et al*. found that their occultation-derived oblateness for Titan's atmosphere, 0.016, implied a supersonic equatorial wind velocity of 340 m s^{-1} if they assumed a global circulation with constant angular velocity, which is how we derived the 290 m s^{-1} value.
18. Winds with speeds exceeding the tangential rotational velocity of the surface have dynamics dictated by the cyclostrophic balance between the force of gravity, the centrifugal force due to the zonal wind circulation, and the pressure gradient force [see J. R. Holton, *An Introduction to Dynamic Meteorology* (Academic Press, New York, 1979)].
19. The altitude of the transition between prolate and oblate isopycs depends somewhat on atmospheric temperature, which was set to 40 K in these models.
20. Altitudes are relative to a spherical surface, assumed to be at the base of the model region, where the pressure is constant. This reference surface need not coincide with Triton's physical surface, so the altitudes of the prolate and oblate regions are adjustable, and the altitude of the reference surface could be different in the northern and southern hemispheres.
21. A. L. Broadfoot *et al*., *Science* **246**, 1459 (1989).
22. V. N. Zharkov, V. V. Leontjev, A. V. Kozenko, *Icarus* **61**, 92 (1985).
23. P. C. Thomas, personal communication.
24. The overlying circular model was derived by decreasing the closest approach distance to create a central flash that was everywhere larger than the oblate model. Using this closest approach distance, we fit a circular model to the oblate model with the central 40% removed (*8*) to match the main drop and recovery of the data. For the IR model, the atmosphere was assumed to be spherically symmetric, with the same atmospheric parameters and closest approach as the overlying circular model. The only source of asymmetry in this model is extinction.
25. J. Hillier and J. Veverka, *Icarus* **109**, 284 (1994).

26. We thank W. McKinnon and P. Thomas for helpful discussions and P. Nicholson and W. Hubbard for comments and criticisms. This work was supported in part by NASA grant NAGW-1494 and by the Friends of Lowell Observatory.

20 December 1996; accepted 22 August 1997